PHYSICAL REVIEW B

CONDENSED MATTER

THIRD SERIES, VOLUME 29, NUMBER 7 1 APRIL 1984

Velocity dependence of secondary-ion emission

M. J. Vasile

AT&T Bell Laboratories, Murray Hill, New Jersey 07974

(Received 23 May 1983; revised manuscript received 21 October 1983)

The emission probability $S^+(v)$ of secondary ions ejected along the surface normal from polycrystalline Cr, Ag, Cu, and Zr is found to be strongly dependent upon the velocity of the secondary ion. The dependence of $S^+(v)$ on the perpendicular velocity component is in qualitative agreement with theories in which the ion formation is governed by a time-dependent perturbation of the outer electronic structure of the atom as it crosses the boundary of the surface into the vacuum. Plots of $\log_{10}S^+(v)$ against v^{-1} show linearity in the energy region $4 \leq E \leq 30$ eV, with slopes of the order of $(2-3)\times 10^6$ cm/sec. Thus exponential dependence of $S^+(v)$ predicted by the time-dependent perturbation theories is observed, at least over a limited energy range. A simple image-force correction extends adherence to linearity below 4 eV, with ion yields as low as 10^{-6}. Positive deviation from the linear dependence of $S^+(v)$ is observed in each case for secondary ions with $E > 30$ eV. This energy region may also be fitted with an exponential dependence of $S^+(v)$, yielding slopes within the range of $(3-6)\times 10^6$ cm/sec.

I. INTRODUCTION

The formation and escape of secondary ions is probably the least well-understood aspect of the sputtering process. Numerous and diverse theoretical arguments have been proposed to explain the phenomenon, but none have been clearly verified by experiment. The emission of secondary ions from clean metal surfaces has been reviewed by Blaise and Nourtier,[1] and Williams[2] has reviewed the topic for ion emission from chemically complex surfaces. Wittmaack[3] has also discussed the subject from a general point of view, and the reader is referred to these articles for exposition and critiques of the specific mechanisms.

The key parameter in all of the theories that have been proposed is the velocity dependence of the secondary-ion emission probability. Measurements of the emission probability as a function of the secondary-ion velocity is the first step necessary to decide which theories are the most promising for further refinement. For example, models based upon local thermodynamic equilibrium (LTE) at the zone of primary-ion impact have a weak velocity dependence for secondary-ion emission probability. Alternative theoretical treatments involving atomic excitation followed by neutralization of the departing ion (either by Auger or resonance processes) predict a very strong velocity dependence for secondary-ion emission probability. Examples of some of these theoretical treatments which represent fundamentally different concepts and some experimental results in accord with each of them follow.

Blandin, Nourtier, and Hone[4] presented a quantum-mechanical treatment in which the excitation of the departing atom is the result of a time-dependent perturbation as the atom moves across the surface boundary. Nørskov and Lundqvist[5] have expanded this treatment and arrive at the following expressions for the positive- and negative-ion emission probabilities $S^+(v)$ and $S^-(v)$:

$$S^+(v)=\frac{2}{\pi}e^{-\pi C_1(I-\phi)/\hbar\gamma v}e^{-\pi C_2/\hbar\gamma v}, \tag{1}$$

$$S^-(v)=\frac{2}{\pi}e^{-C_1\pi(\phi-A)/\hbar\gamma v}e^{-\pi C_2/\hbar\gamma v}. \tag{2}$$

C_1 and C_2 are constants in a linear interpolation scheme which accounts for the variation in the effective difference between the ionization potential (or electron affinity) and the Fermi energy, as the particle moves outward from the surface. γ is a characteristic distance beyond which no further electron exchange between the atom and the substrate takes place, and v is the perpendicular component of the particle velocity. (The symbol v will always refer to the perpendicular velocity component in the remainder of this paper.) The velocity dependence is clearly strong. As v decreases to the extent that the ion energy is of the order of the image potential, the ion emission goes to zero; as v becomes large, the ion emission probability should approach a value of $2/\pi$. The logarithm of $S(v)$ should also be a linear function of $1/v$ with the slope given by the constants C_1, C_2, γ, and the value of $I-\phi$ or $\phi-A$.

Experimental evidence in support of these predictions has appeared in the recent literature. Yu[6] has recently

shown that emission of O^- from oxygen chemisorbed on vanadium and niobium has an exponential dependence on velocity for $v > 1\times10^6$ cm/sec ($E > 8.4$ eV) and that the work function dependence is also in accord with Eq. (2). Lang[7] has expanded upon the theory of Nørskov and Lundqvist to account for most of the experimental observations of Yu. The situation for positive ions is somewhat less encouraging. Several attempts to extract an $\exp(-C/v)$ velocity dependence [with $C=A/a$ from Auger neutralization theories, or $\pi C_1(I-\phi)/\hbar\gamma$ from resonance neutralization theories], have met with no success,[8] or only very limited success.[9,10] Recently this author[11] has published data which show a linear dependence of $\log S^+(v)$ over several decades for Cu^+ ejected from single-crystal copper.

An alternative theoretical description of secondary-ion emission has been worked out by Sroubek *et al.*[12–14] Electronic excitation within the collision cascade region is described in terms of an effective temperature T_s with a probability proportional to $\exp(-\epsilon/kT_s)$. Early results based on this model predicted a very weak velocity dependence for the secondary-ion emission probability.[13] Recent refinements of this approach include the interaction of the ejected atoms with the excited substrate, which results in a velocity dependence in the exponential term. The velocity dependence is introduced through the time variation of the valence level of the ejected atom $\epsilon_a(X_0)$, in the expression $S^+=\exp\{[\epsilon_F-\epsilon_a(X_0)]/kT_s\}$, with $\epsilon_a(X_0)$ proportional to $\ln(C/v)$. Calculations predict a factor of 5 (Ref. 14) increase in the secondary-ion yield for copper over the energy range of 4 to 40 eV, which is a much weaker velocity dependence than predicted by expressions such as Eq. (1).

Experimental evidence in support of a weak velocity dependence for $S(v)$ has also appeared in the recent literature. Gibbs[15,16] *et al.* have reported experiments involving the ejection of Ni^+ from a $c(2\times2)$CO overlayer on Ni(001) as a function of polar angle and particle energy. The experimental Ni^+ angular distributions and kinetic energy distributions were compared to the corresponding neutral distributions predicted by their classical dynamics calculations. Correlations between the predictions for neutral particles and the experimentally observed ions were obtained after image-force corrections were made. These authors conclude from the observed correlations that ion emission from a Ni(001)-$c(2\times2)$CO surface is isotropic and only weakly dependent upon the ion velocity. The Ni^+ ion yield is enhanced by a factor of 10^4 over that of a clean Ni surface under these conditions,[17,18] and this fact must preclude the generalization of their observations to clean surfaces. Gibbs[15,16] *et al.* also report no success in obtaining correlations between an $\exp(-C/v)$ velocity dependence between the observed ion kinetic energy distribution from clean nickel surfaces and their calculated neutral energy spectrum, except at a polar angle of 30°.

Thus we have at least two fundamentally different concepts of the secondary-ion emission process, and some experimental evidence that supports or correlates with each of them. There is clearly a need for further experiments to give a more definitive test to these theories. The basic problem addressed in this study is the velocity dependence of the emission probability of positive secondary ions that are ejected from transition-metal surfaces. The main question is whether or not we observe strong velocity dependences of the ion-emission probability from clean metal surfaces in an ultrahigh vacuum.

II. EXPERIMENTAL CONSIDERATIONS

A. Experimental requirements

The difficulties encountered in obtaining even rudimentary agreement between theory and experiment in secondary-ion emission are formidable. Quantum-mechanical treatments of excitation and neutralization of a sputtered particle as it leaves the surface are extremely complex; approximations must be made to obtain relationships which can be experimentally tested. The relevance of the experimental test is therefore only valid within the accuracy allowed by the approximations in the theory. The chemical environment or state of the surface is a critical parameter: Ion yields can vary over several orders of magnitude with the presence of adsorbed species.[19] The energy spectrum of sputtered neutrals is also a fundamental issue. The closed-form equations for the Sigmund-Thompson treatment[20–22] are convenient to use and have been experimentally verified for a few polycrystalline metals with low primary-ion energies.[23–25] The validity of the calculated energy spectrum for atoms sputtered with energies greater that ~30 eV remains to be checked, especially for primary ions with energies as low as a few kilovolts. The sputtering yield in this energy region has been shown to be greater than predicted by the collision-cascade model, mainly as a result of direct or deflected surface recoils.[26] The increase, however, is the least pronounced for particles leaving along the surface normal.

Instrumental and geometric difficulties compound those mentioned above. A test of the velocity dependence of the secondary-ion emission requires that we know the ion current relative to the total particle current over a given velocity range. We must further know these quantities at a point above the surface where all excitation and neutralization events are over. The collision-cascade treatment can be used to account for the sputtering of atomic particles from polycrystalline solids, but the primary ions must strike the surface at normal incidence in order to minimize any contributions of direct surface collisions to the sputtered particle population.[26] Energy analysis of the secondary ions originating from a well-defined angle with respect to the surface must also be performed. These restrictions are not simple to achieve with conventional secondary-ion mass spectrometers (SIMS).

The transmission of the measuring instrument must also be known as a function of ion energy, if we are to remove distortion introduced by the measurement. Most of the earlier measurements which provided data relevant to the theory of secondary-ion emission were taken with instrumental arrangements that did not satisfy these criteria. Only recently have these necessary features been incorporated into experimental configurations[27,28] which are designed primarily to study the ion-emission process, rath-

er than to obtain intense secondary-ion signals for optimum SIMS analyses.

The experiments in this study are specifically designed to conform to the conditions stated previously: (1) normal primary-ion incidence, (2) limited secondary-ion acceptance angle, (3) measured transmission characteristics of the energy/mass filter, and (4) use of polycrystalline substrates.

B. Apparatus and procedures

The basic arrangement of the apparatus used in this study provides a low kinetic energy (0.5—3 kV), low current density (3×10^{-8} A/cm^2) argon-ion beam at normal incidence to the surface. Secondary ions are extracted in the normal direction into a resistive disk energy filter which is mated to a quadrupole mass filter. A complete description of this unique instrument and the analysis of ion trajectories through it are given in Ref. 28.

The analyzer chamber was pumped to 5×10^{-8} Pa and the primary-ion chamber was pumped to 6×10^{-7} Pa after baking. A titanium sublimator and a turbomolecular pump were used during secondary-ion measurements; the analyzer chamber pressure rose to 3×10^{-6} Pa due to the effusion of argon from the primary-ion chamber.

Secondary-ion measurements were made with a 2-kV primary-ion beam at a current density of 3×10^{-8} A/cm^2 [0.1-cm-radius full width at half maximum (FWHM) ion beam]. Initial sputtering of the surfaces was done with a 3-kV ion beam at a current density of 1.5×10^{-7} A/cm^2, using a 0.2-cm-radius ion beam (FWHM). Exposure of the samples at elevated temperature to carbon monoxide[29] was also used in addition to sputtering to remove surface oxide. Targets for secondary-ion emission were polycrystalline samples of Cu, Ag, Zr, and Cr, with quoted total purities of 99.999%, 99.999%, 99.98%, and 99.95%, respectively. The Cu, Zr, and Ag were foils, while the Cr was in the form of a lump which was subsequently machined into a planar segment. The surfaces of each specimen were polished to a mirror finish prior to chemical etching, methanol rinse, and mounting.

C. Transmission-calibration techniques

The transmission calibrations are an essential part of the procedure in this study. A transmission function for the instrument used in this study was analytically derived in Ref. 28. The essential features of the transmission characteristics were previously tested, but a more systematic calibration of the transmission was necessary. These calibrations were done with a thermal ionization source of K^+ or Rb^+ ions. This source consisted of a resistivity heated tungsten ribbon (1 mm wide$\times$0.025 mm thick) mounted inside a stainless-steel envelope with a 2-mm-diam hole in it. The potential of the filament was raised to the desired ion energy, while the potential of the surrounding envelope was fixed. This ion source was mounted on a precision rotary-linear motion feedthrough, and it simply replaced the target assembly used in the secondary-ion measurements. The geometric and electrostatic arrangement ensured that the thermally generated ions originated from a locus identical to that of the secondary ions. Measurement of the ion current was achieved by rotating the source through 90° to face a screened collector. Retarding potential measurements provided the energy distribution of the thermally generated ions at each setting of the ion energy. These ion-current measurements were made before and after each transmission measurement. Saturated solutions of KCl or RbCl were evaporated from the tungsten ribbon at room temperature prior to mounting this source on the vacuum system. During the initial operation of the thermal-ion source, the mass spectrum of the thermally generated ions was monitored (prior to the calibration measurements) until a pure-ion beam of either K^+ or Rb^+ was obtained. Calibration ion currents of $(1-3)\times10^{-12}$ A were measured using a current-to-frequency converter and pulse counting (minimum current of 1×10^{-14} A).

D. Transmission measurements

1. *Energy dependence*

Secondary-ion signals measured at any energy are a convolution of the instrument transmission and the kinetic energy distribution of the ions. The latter quantity is broad, with a long high-energy tail, so the bandwidth variation of the energy filter must be incorporated into the transmission measurements. This was accomplished since the energy spread of the thermally generated ions is narrow relative to the bandpass of the energy filter. A nominal fixed energy E_1 was set for the ions generated by the thermal ionization source, and the acceptance energy of the energy filter was swept over its bandpass ΔE in incremental steps δE_n. A mass-analyzed current N_n^+ was recorded at each incremental energy step, and the sum $\sum_n N_n^+ \delta E_n$ computed. The transmission over the energy bandpass ΔE at nominal energy E_1 is then

$$T(E)=\sum_n N_n^+ \delta E_n \Big/ \left[N_K^+ \sum_n \delta E_n \right], \tag{3}$$

where N_K^+ is the ion current of K^+ incident at the energy-filter aperture. Figure 1 shows the K^+-ion current measured versus the energy-filter settings for a nominal 50-V energy. The energy spread of the K^+-ion beam is superimposed. The data are normalized to the maxima for convenience of display; the actual transmission value is 2×10^{-3}. The bandwidth of the instrument transmission is 6.5 eV at the half maximum point, and the predicted[28] half-width based on the analytically derived transmission function at this energy is 9.4 eV.

The process of measuring the bandwidth-corrected transmission outlined above was repeated for nominal energy settings over the range from about 3 to 60 eV. The results are shown in Fig. 2. The energy dependence of the transmission was best fit by the equation $T(E)=0.2/E^{1.25}$, shown as the solid curve. This expression gives values of $T(E)$ well within the bounds of the error estimates of the measured points, over the entire energy range. Figure 2 also includes a transmission curve calculated from the analytically derived $T(E)$ given in Ref. 28. The qualitative agreement in the functional dependence provides some confidence in the $S^+(E)$ results previously

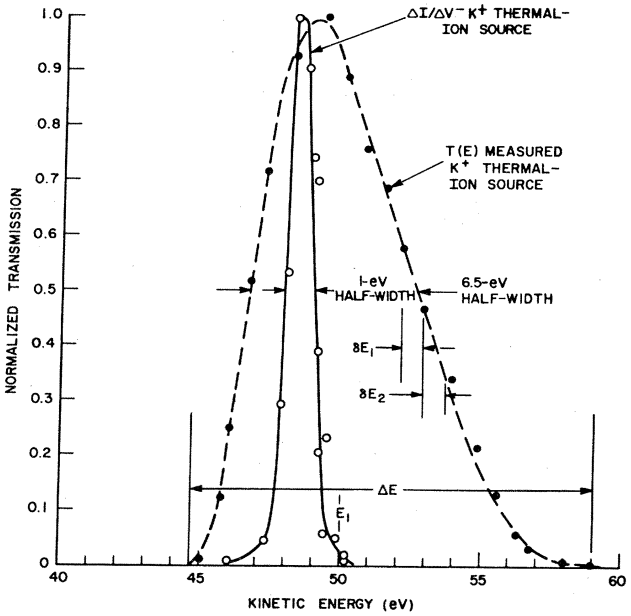

FIG. 1. Dashed curve is a plot of the normalized transmission of the instrument obtained at a nominal energy E_1 of 50 eV using the K^+ thermal-ion source. The peak transmission value is 2×10^{-3}; the energy spread of the K^+ ions is shown superimposed as the solid curve. The bandpass of the energy filter is shown as ΔE, and incremental steps in acceptance energy are shown as δE_1 and δE_2.

obtained[11] using the analytically derived transmission function.

2. Angular dependence

The angular acceptance of the instrument was checked by rotating the thermal-ion source in 0.5° increments, to provide ions with off-normal velocity components (with respect to the plane of the energy-filter aperture). A bandwidth-integrated transmission was measured at each angle. Results for a Rb^+-ion beam at nominal energy of 20 eV are shown in Fig. 3. The transmission is normalized to the maximum value (5×10^{-3}), and it is a much sharper function than the original estimate[28] of a maximum 12° off-normal component. This is clearly a benefit, since secondary ions with values of $\phi > 3°$ will not be transmitted, and corrections of the measured ion currents for off-normal components are negligible.

3. Mass and resolution dependence

The resolution dependence was measured at a few energies by purposely offsetting the resolution control of the mass filter. A curve of transmission versus Δm FWHM was generated, and found to be a weaker function than the $(\Delta m)^2$ term in Ref. 28. The $1/m$ mass dependence is adequate as can be seen from the Rb^+ points on the $T(E)$ plot in Fig. 2.

To summarize the results of the transmission measure-

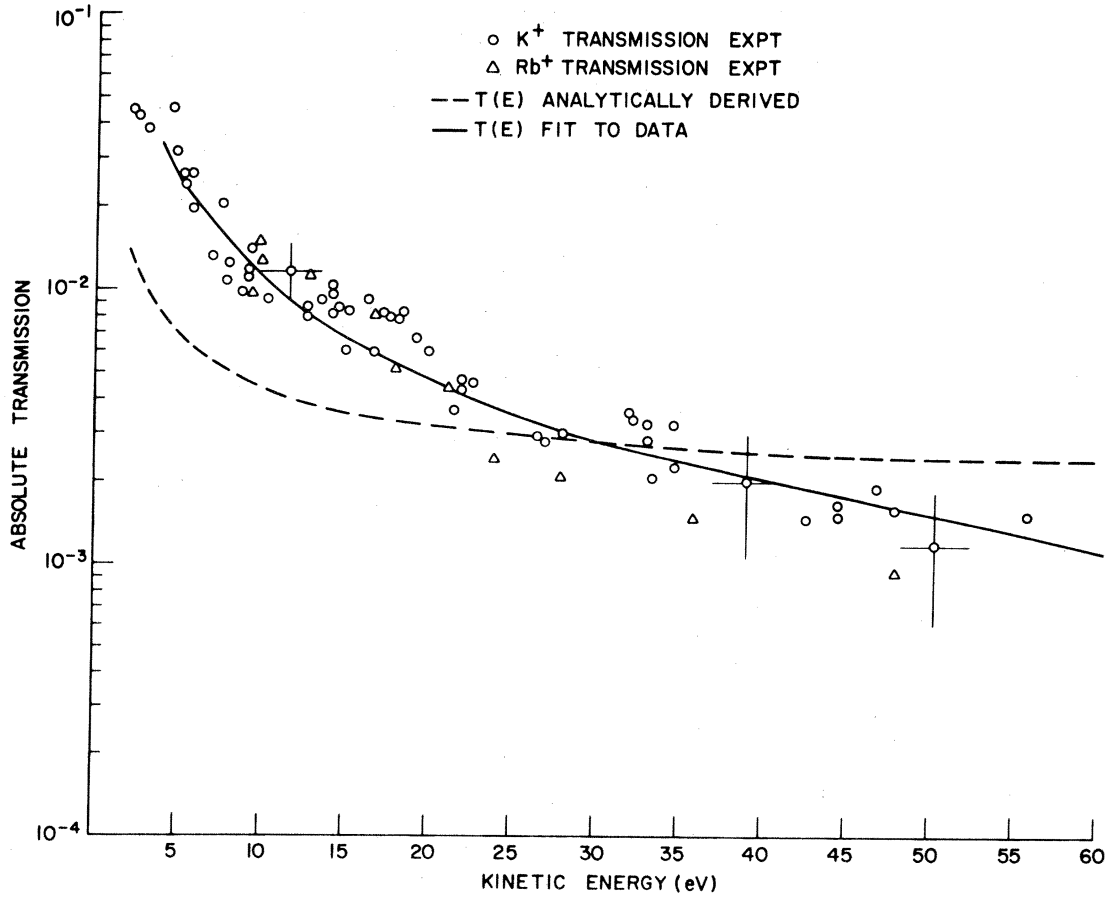

FIG. 2. Bandwidth-integrated transmission data taken over the energy interval $3 \le E \le 55$ eV, using either a source of K^+ or Rb^+ ions. The solid curve is the $T(E)=0.20/E^{1.25}$ dependence, and the dashed curve is the analytically derived transmission function used previously (Ref. 28).

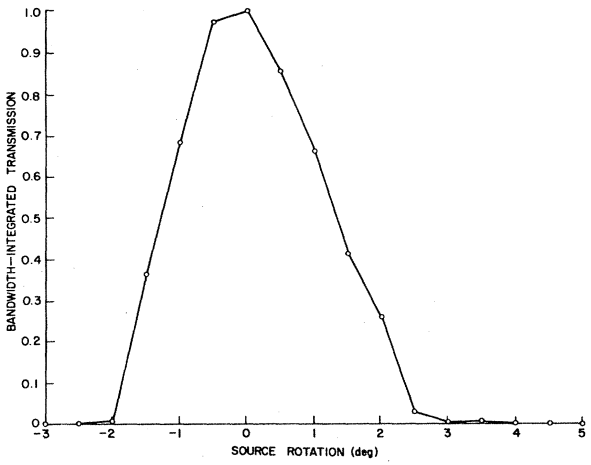

FIG. 3. Bandwidth-integrated transmission measurements for ions entering the energy filter with off-normal angles.

ments, relative to the analytically derived function,[28] we find the following: (1) The energy bandwidth of the instrument is narrower than predicted, (2) the angular acceptance is much more restrictive to normally incident ions, (3) the mass dependence of $1/m$ is adequate, (4) the absolute transmission is higher than predicted for ion energies less than about 20 eV, and (5) the resolution dependence is weaker than expected. The corrections dictated by the transmission calibrations were incorporated into a computer program using closed-form equations. Ion currents measured at any arbitrary energy could then be transformed back into the normal component of the ion current above the solid surface.

III. RESULTS AND DISCUSSION

The secondary-ion emission probability at any given energy is defined by Eq. (4):

$$S^+(E)=N^+(E)/N_0(E)\ , \tag{4}$$

where $N^+(E)$ is the rate of ion ejection at energy E, and $N_0(E)$ is the rate of atomic-particle ejection along the normal to the surface. $N^+(E)$ symbolizes the ion-ejection rate above the surface at a point where no further electronic interactions take place. $S^+(E)$ is then the fraction of atomic particles sputtered along the surface normal with energy E, which escape the surface in the positively charged state.

We measure $N^+(E)$, and for the purposes of this study, we calculate $N_0(E)$. The energy distributions of particles sputtered from three of the target materials (Cu, Ag, and Zr) used in this study have been shown to conform[23–25] to the Sigmund-Thompson relationship.[20–22] We then write the probability of an atomic particle being ejected at energy E and angle ϕ as

$$P(E,\phi)=\frac{AE}{(E+E_b)^3}\cos\phi\ , \tag{5}$$

where ϕ is the angle of ejection with respect to the surface normal, E_b is the surface binding energy, and A is a constant evaluated from the requirement that the integral of $P(E,\phi)$ over all directions and energies is unity. The rate at which atomic particles are ejected N_0 is given by the primary-ion current I_0^+, and the sputtering yield Y, for the combination of the target material and the primary-ion mass and kinetic energy:

$$N_0=I_0^+Y\ . \tag{6}$$

These sputtered particles are distributed in energy and space by the product of Eqs. (5) and (6):

$$N_0(E,\phi)=I_0^+Y\frac{2E_b}{\pi}\frac{E}{(E+E_b)^3}\cos\phi\ , \tag{7}$$

where E_b is approximated in this study by the cohesive energy of the solid.

The rate of ejection of positive ions $N^+(E)$ from the surface is proportional to the measured ion count rate, $N_m^+(E)$. The relationship between the measured count rate (after the ions transit through the instrument) and the rate of ejection of ions from the surface must be known to compute $S^+(E)$ from Eq. (4). The transmission measurements show that this relationship, $T(E,\phi)$, is a function of the ejection angle ϕ, the ion energy E, the ion mass, and the resolution of the mass filter. For a given target and fixed-mass resolution we have, for $\phi=90°$.

$$N^+(E)=N_m^+(E)/T(E,90°)\ . \tag{8}$$

Since $T(E,90°)$ is known, the measured ion currents may be converted to $N^+(E)$, and $S^+(E)$ may be calculated via Eqs. (7) and (4).

The sensitivity of the ion fraction, and its velocity dependence to the functional form of calculated neutral particle ejection rate, Eq. (7), can be tested. The exponent in the energy term $E/(E+E_b)^3$ may be varied over the range which has been observed experimentally,[25] and the effect of variation of E_b may also be conveniently examined. Secondary-ion current measurements are restricted to an angular spread of about $\pm2°$ from the surface normal (cf. Fig. 3). An angular distribution function other than $\cos\phi$ in Eq. (5) (e.g., $\cos^2\phi$) would alter the results obtained in this study (at $\phi=90°\pm2°$) only through the value of the normalization constant, A.

A. Secondary-ion emission

1. *Targets*

Copper, silver, and zirconium were chosen as substrates for a range in ionization potentials, and because independent measurements[23–25] show that the energy spectrum of particles sputtered by low-energy primary ions conforms well to Eq. (5). Chromium was included with zirconium as a second low-ionization potential element, even though the energy spectrum of its sputtered particles has not been measured. The choice of substrates also provides considerable variations in binding energies and sputtering yields, as summarized in Table I.

2. *Secondary-ion spectra*

Low-energy secondary-ion currents decreased significantly (by a factor of 50 to 100) on Cu, Ag, and Zr when

TABLE I. Binding energies, sputtering yields, and ionization potentials of the target metals in this study.

Element	Binding energy[a] (eV)	Sputtering yield[b] (atoms/ion)	Ionization potentials (eV)
Cu	3.5	4.0	7.68
Ag	2.96	5.5	7.54
Zr	6.32	1.2	6.92
Cr	4.10	2.0	6.74

[a]Cohesive energy of the solid.
[b]Taken from Ref. 37, for 2-kV argon ions at normal incidence.

the surface was cleaned by sputtering and CO reductions. The decrease on copper reproduced previously observed data,[11] and the decrease on chromium was the smallest for these targets (by a factor of 10). The reduction in low-energy ion population produces a shift in the energy distributions toward higher energy,[11] but the shifts observed are not as pronounced as those reported by Snowdon and MacDonald.[30] When the Cr^+, Cu^+, and Ag^+ ion currents were at their lowest, steady-state values (10^3, 600, and 300 counts/sec), count rates from ions such as Ag_2S^+, $AgCO^+$, Cu_2O^+, and $CuCO^+$ were at the background count level (1 count/2 sec). A small CrO^+ peak (1% of the Cr^+ intensity) could be detected. Zr^+ and ZrO^+ were the exception to this behavior. Initially the low energy ZrO^+ and Zr^+ signals were essentially equivalent, at about 3×10^4 counts/sec. Sputtering and CO reductions reduced the count rates of both of these peaks significantly, but ZrO^+ could still be detected at ~10 counts/sec.

Energy spectra of the secondary ions for each of the targets obtained under the cleanest surface conditions possible are shown in Fig. 4. These spectra are broad (i.e., relatively high fractions of ions with energies greater than about 20 eV) when compared to some published spectra (e.g., the Cu^+ spectra in Ref. 31); however, the shape of the observed energy spectrum of secondary ions has been shown to be a function of ion extraction conditions,[32] and it is also a function of the presence or absence of absorbed gases.[11] Correction of the data in Fig. 4 for instrument transmission yields energy spectra with strong qualitative resemblance to those obtained by Bayley and MacDonald,[32] who also employed an instrument transmission correction.

3. *Ion emission probability as a function of velocity*

The ion fraction of sputtered particles $S^+(v)$ was computed as a function of velocity on a point-by-point basis, using Eqs. (8), (7), and (4). The measured ion count rate after transmission correction and the computed sputtered particle count rates should give a close approximation to absolute results. The ion fractions, $S^+(v)$ plotted on a log scale against the inverse velocity, are shown in Figs. 5–8. In each plot the open circles are obtained without an

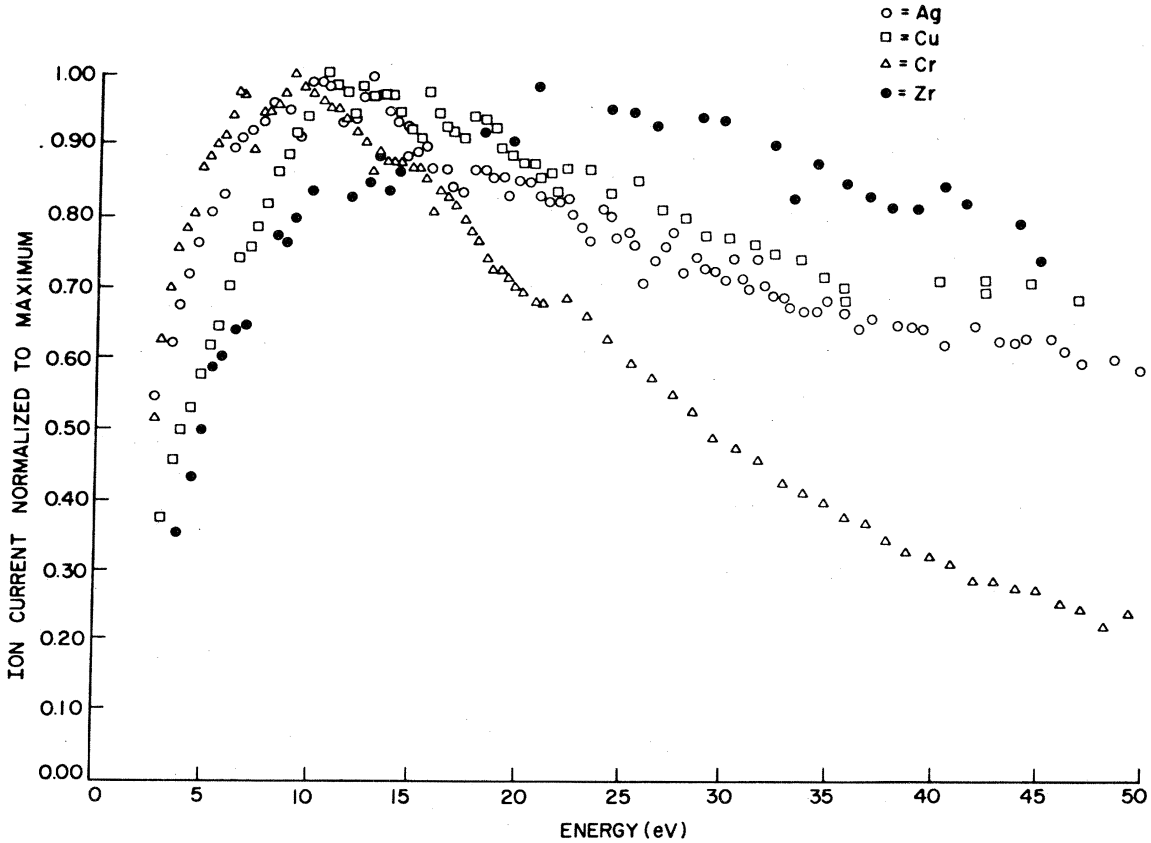

FIG. 4. Secondary-ion energy spectra for Cu^+, Ag^+, Cr^+, and Zr^+ normalized to the maximum count rate under the cleanest surface conditions achievable.

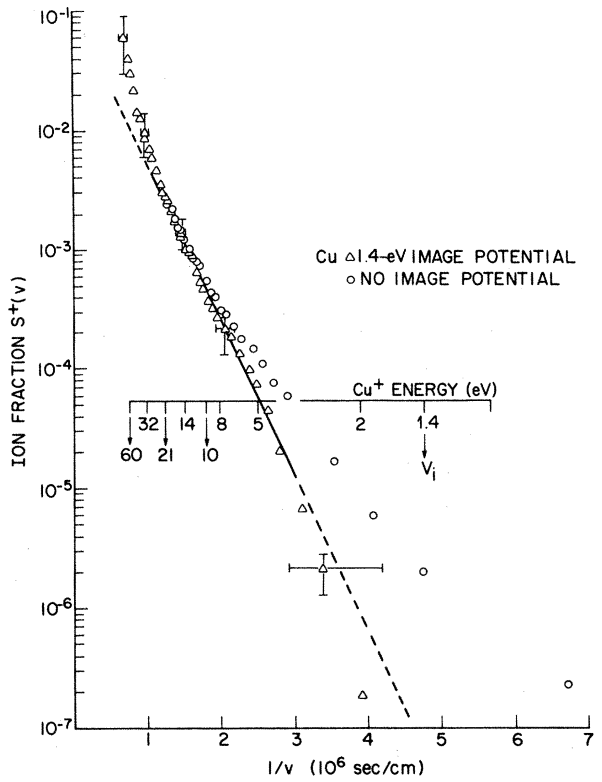

FIG. 5. A plot of $\log_{10}S^+(v)$ vs v^{-1} for Cu^+. Open circles are data without the 1.4-eV image-force correction, and the triangles are data with the image-force correction. The solid line was obtained by a linear regression, the dashed lines are extrapolations beyond the last points used in the regression.

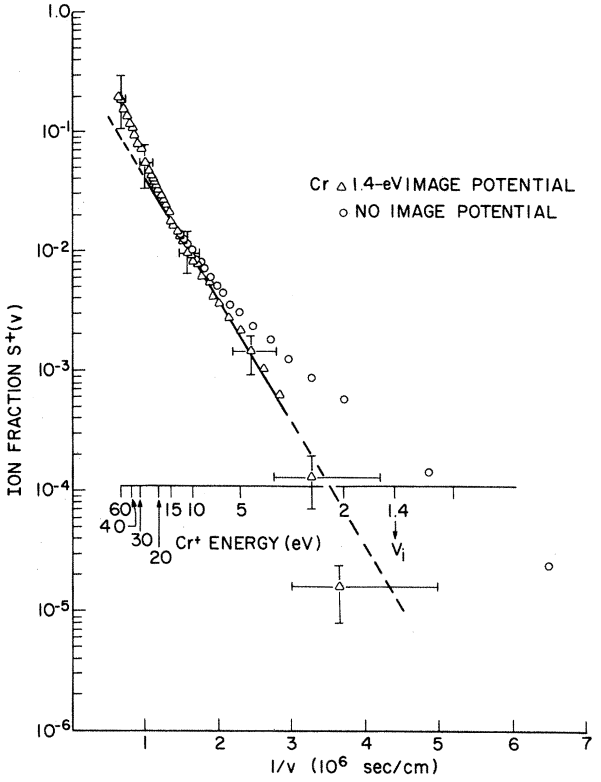

FIG. 7. A plot of $\log_{10}S^+(v)$ vs v^{-1} for Cr^+. Symbols have the same meaning as in Fig. 5.

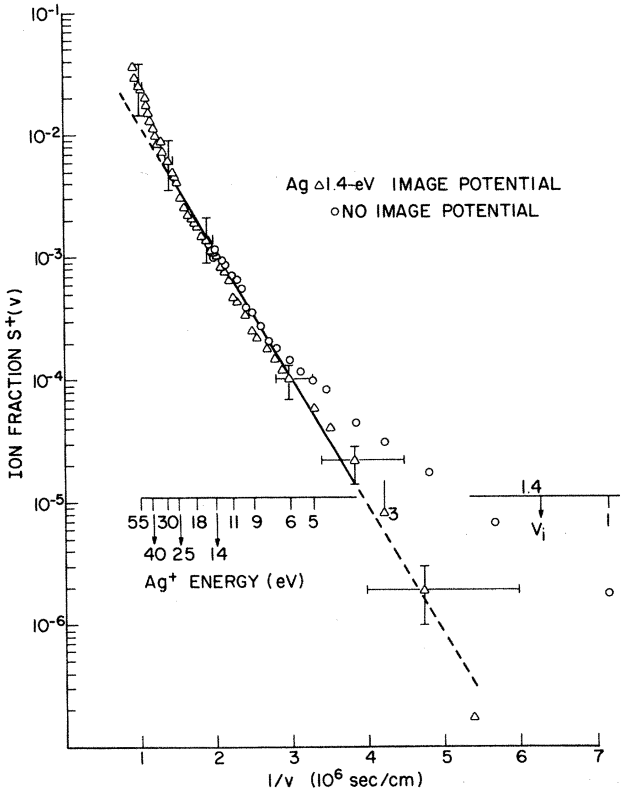

FIG. 6. A plot of $\log_{10}S^+(v)$ vs v^{-1} for Ag^+. Symbols have the same meaning as in Fig. 5.

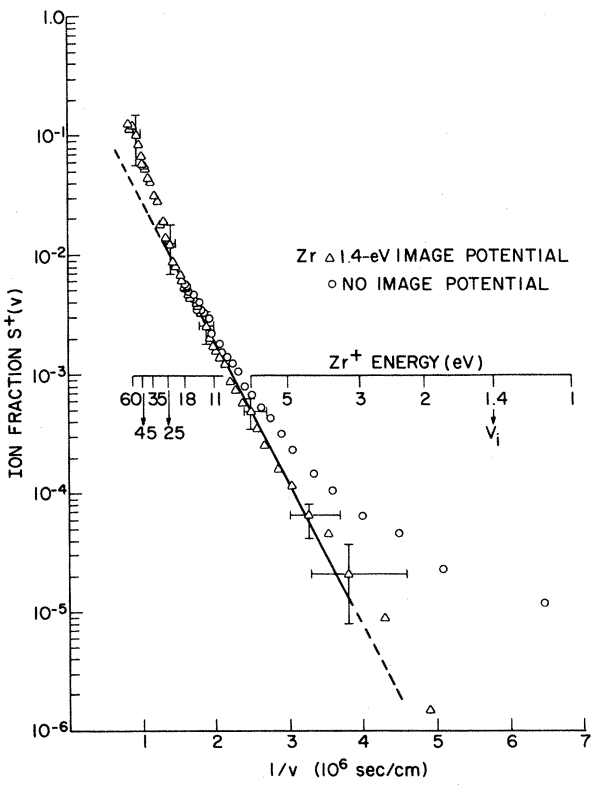

FIG. 8. A plot of $\log_{10}S^+(v)$ vs v^{-1} for Zr^+. Symbols have the same meaning as in Fig. 5.

image-force correction (which will be discussed subsequently), and the triangles are the values obtained after applying the image-force correction. Error bars shown at different orders of magnitude of $S^+(v)$ are compounded from errors in the transmission correction, the count rate, and the uncertainty in the energy axis.

Each of the plots has a straight line segment fitted by linear regression over the energy interval of ~ 4 to ~ 30 eV. We defer discussion of these straight-line fits until after more fundamental implications of the data are considered.

The secondary-ion fractions obtained in this study are obviously very strongly dependent upon the secondary-ion velocity. Examination of Figs. 5–8 shows that $S^+(v)$ for Cr^+ and Zr^+ ranges over at least 4 orders of magnitude and $S^+(v)$ for Cu^+ and Ag^+ varies over at least 5 orders of magnitude. The ranges of $S^+(v)$ referred to in the latter statement are for the values without image-force corrections. Inclusion of the image force extends the range in $S^+(v)$ to between 5 and 6 orders of magnitude. Sroubek's treatment[14] predicts an order-of-magnitude increase in $S^+(v)$ of Cu^+ over the energy range from 4 to 60 eV, while the data in Fig. 5 show an increase of approximately 3 orders of magnitude. Thus we observe a much stronger velocity dependence than predicted by the theory of Sroubek,[14] but it is in qualitative accord with the theories proposed by Blandin, Nourtier, and Hone,[4] and Nørskov and Lundqvist,[5] which predict $S^+(v)\rightarrow 0$ as $v\rightarrow 0$ and $S^+(v)\rightarrow 0.6$ as $v\rightarrow\infty$.

The effect of the image-force correction is to remove the "tailing off" of $S^{(+)}v$ at low velocity, which may be interpreted[8] as an emission probability for zero-energy ions. The image-force correction was arrived at using the framework of the theory of Nørskov and Lundqvist, in which they estimate the image potential V_i at a distance from the surface where all the overlap effects with the substrate electrons have disappeared. We assume that any ion ejected with energy less than the value of the image potential at the point above the surface where electron exchange ceases will be neutralized. This means that the observed ion-energy scale begins at V_i, relative to the energies of the ions ejected at the surface. Nørskov and Lundqvist[5] deduce a value of 1.4 eV for Cu^+ ejection using the analysis of Sidyakin,[33] and further argue that the image-force effect will have a weak dependence on the material, so a 1.4-eV correction was applied to each of the sets of data. With the use of this correction, we see that the value of $S^+(v)$ decreases rapidly as the value of the image-force potential is approached. The uncorrected and corrected data also merge as the energy of the ion becomes large with respect to the value of the image-force potential.

4. *The exponential dependence of* $S^+(v)$

A strong velocity dependence of S^+ is observed for each of the materials, with the qualitative features expected from either Nørskov and Lundqvist's treatment, or from the Auger neutralization of an outgoing charged particle.[34] We are therefore obliged to examine the results in more detail. The values of the slopes of the linear segments for each of the elements, and the values of the ion fractions at any given velocity are important parameters relating to these theories of ion emission. We must recognize, however, that due to the inherent complexity of this problem, a detailed analysis of these results will only indicate a direction for further theoretical and experimental work.

The exponential dependence consists of two distinct segments after correction for the image force. The segments from 30 to 4 eV were fitted to a linear dependence, and extrapolations of this line to higher and lower energies are shown by the dashed segments. The lower-energy limit in the fitting was chosen since this is the lower limit of the transmission measurements, and it is also near the maximum in the sputtering function for most of the materials, $E_b/2$. Equation (5) is likely to be less reliable in predicting $N_0(E)$ near the maximum $(E_b/2)$ due to thermal spike effects than it will be in energy range of about 5 to 25 eV. The high-energy limit in the regression analysis was chosen at 30 eV since deviations begin here, and also because experimental verifications of $N_0(E)$ do not extend beyond about 25 eV. Note that the extrapolated linear segments fit the data quite well within the experimental error at low energies. Thus good adherence to an $\exp(-C/v)$ relationship holds for each material over four or five decades, once a simple image-force correction is made.

Next we consider the magnitudes of the slopes obtained between 4 and 30 eV in relation to what can be expected from theory. Again, caution must be used since we shall be comparing the slopes of $\log_{10}S^+(v)$ for different materials. These slopes are obtained on the premise that the exponent n in the neutral atom sputtering function is 3.0 for each of these materials, and on the premise that E_b is adequately represented by the cohesive energy of solid, rather than the surface atom binding energy. Tests for the sensitivity of the exponential dependence of $S^+(v)$ were done by independently varying these parameters. A binding-energy range for copper from 3.0 to 4.0 eV did not change the fundamental result: The exponential dependence of $S^+(v)$ remained, and the values of the slopes obtained ranged only from 2.9×10^6 to 3.1×10^6 cm/sec. Wright *et al.*[25] found $n=2.85\pm 0.15$ as the exponent for the sputtering function for Zr with $E_b=6.31$ eV. The exponential dependence of $S^+(v)$ was again unchanged by the substitution of $n=2.70$, and 2.85 into Eq. (7) for the analysis of the zirconium data. The values of the slopes obtained varied only between 2.3×10^6 and 2.6×10^6 cm/sec. It is of interest to note that the best fits for these linear regression sensitivity tests occurred with the value of E_b at the cohesive energy, and with the value of the exponent $n=3.0$.

Nørskov and Lundqvist's theory predicts the slope of $\log_{10}S^+(v)$ vs $1/v$ for the metal ion sputtered from the solid to be

$$\frac{\pi C_1}{\hbar\gamma}(I-\phi+V_i)\ .$$

The same image-force correction V_i was applied for each of the materials in this study, so the slopes should vary as $C_1(I-\phi)/\gamma$. The principal variation[5] should arise from

the $(I-\phi)$ term, but we cannot expect more than a correlation with this parameter. A complete numerical solution of the electron occupancy as a function of time for each material with the appropriate dependences of C_1, γ, and V_i is necessary for a detailed comparison.[5]

The measured values of the slopes and the measured values of the ion fractions at an arbitrarily chosen velocity of 5×10^5 cm/sec are listed in Table II. There is no correlation with the parameter $(I-\phi)$ when ϕ is determined from the photoelectric effect on polycrystalline substrates[35] (column A). The relevance of work function in the secondary-ion emission problem has been appropriately questioned,[2] since the atoms in the lattice from which the sputtered particle departs are severely displaced, and in motion. A closer approximation to the work function at the site of the collision cascade might then be the thermionic work function. The values of $(I-\phi)$ based on the thermionic work function are therefore included in Table II, and we see that there is only 0.5 eV spread in values, which is at least in qualitative agreement with the small variation in the slopes obtained from $\log_{10}S^+$ versus 1/v plots. In view of the premises upon which these $\log_{10}S^+$ plots were obtained, we cannot expect much better than this correlation.

Each of the plots shows a break at approximately 30 eV, with a positive deviation in $\log_{10}S^+(v)$ relative to the extrapolation of the linear fit. These high-energy data may also be fitted with straight lines, yielding slopes of $\ln S^+(v)$ which range between 5.7×10^6 cm/sec for Cu^+, and 3.2×10^6 cm/sec for Cr^+. Yu reports an exponential dependence of S^- on $1/v$ with a slope[6] of 5×10^6 cm/sec, for O^- emission from oxygen adsorbed on vanadium and niobium. This behavior is observed for O^- velocities greater than 1×10^6 cm/sec, which is precisely the region where the high-energy segments are observed in this study. It is tempting to cite a correlation here, especially with regard to the magnitude of the slopes, but we must bear in mind that the correlation is between the ionization probability of a sputtered adatom and that of a sputtered lattice atom.[7]

In addition to an enhanced sputtering yield[26] in this energy region, there is also a possibility that the increased ion yield at $E>30$ eV is a result of small deflections of the primary-ion beam onto the periphery of the sputtered zone, where the ion yield is enhanced. Deflection of the primary-ion beam can occur due to the geometry and the energy filter used in this experiment. Strong radial electric fields are necessary for selection of secondary ions with energies greater than about 30 eV. Unfortunately, the magnitude of the deflection of the primary-ion beam by these radial electric fields is difficult to estimate. Further experiments are therefore necessary to determine whether the functional dependence of $S^+(v)$ observed at $E>30$ eV is real. A true two-segmented linear dependence of $S^+(v)$ compounds theoretical difficulties.

The values of the ion fractions listed in Table II order with the ionization potential, i.e., the ionization probability increases as the ionization potential decreases. It is difficult to see how these ion fractions can order in such a way within the framework of Nørskov and Lundqvist's theory, since a stronger divergence with $1/v$ is necessary. In other words, the observed variations in the slopes of $\ln S^+$ listed in Table II are not large enough to produce the range in ion fractions at $v=5\times10^5$ cm/sec, if these lines radiate from a common velocity $(v=\infty)$ at $S^+=2/\pi$. The answer to this dilemma may come from a more thorough experimental investigation of the observed high velocity $(E>30$ eV) component to the ionization probability, and a better accounting for the binding energy of departing ion to the surface.

IV. SUMMARY

We observe a strong velocity dependence of the secondary-ion emission probability for four different transition metals. Within the limits of the approximations which have been previously discussed, the qualitative behavior of the velocity dependence of $S^+(v)$ is in agreement with the time-dependent perturbation analysis given by Blandin, Nourtier, and Hone,[4] and by Nørskov and Lundqvist.[5] It is also consistent with the general behavior of Auger neutralization theory, in that an $\exp(-A/av)$ relationship holds for the survival probability of the departing ion. The Auger neutralization mechanism has frequently been invoked in descriptions of the sputtering of excited or ionized particles, but the theory has only been worked out in detail for the combination of rare-gas ions (or metastable excited states) with metallic surfaces.[34,36] A detailed treatment of the Auger neutralization of a metal ion departing from a metal surface is required to assess whether the results of this study fit Auger neutralization or time-dependent perturbation phenomena more accu-

TABLE II. Slopes of $\ln S^+(v)$ vs v^{-1} and ion fractions. Column A is based on photoelectric work functions (Ref. 34) measured on polycrystalline specimens in ultrahigh vacuum. Column B is based on selected values of thermionic work functions (Ref. 34) and references contained therein.

Element	Slope[a] (cm/sec)	$I-\phi$ A	$I-\phi$ B	Ionization potential	Ion[b] fraction
Cu	3.0×10^6	3.0	3.3	7.68	3×10^{-4}
Ag	2.4×10^6	3.5	3.2	7.54	1×10^{-3}
Zr	2.6×10^6	2.9	3.0	6.92	2×10^{-3}
Cr	2.3×10^6	2.2	2.8	6.74	4×10^{-3}

[a]For the energy range $4\leq E\leq30$ eV.
[b]Taken at $v=5\times10^5$ cm/sec.

rately.

Further refinements in the experimental treatment are also necessary. The reason for the break in the linear relationship for $E > 30$ eV should be found. A better approximation to the surface binding energy and further verification of the sputtering relationship would be of extreme value when attempting to compare ion yields of one material to another.

ACKNOWLEDGMENTS

The author would like to acknowledge Mr. Jeffrey Tolk for his part in taking much of the experimental data, and for writing many of the computer programs necessary. Mr. J. C. Tully is also acknowledged for his stimulating and challenging discussion, throughout the course of this work.

[1]G. Blaise and A. Nourtier, Surf. Sci. 90, 495 (1979).
[2]P. Williams, Surf. Sci. 90, 588 (1979).
[3]K. Wittmaack, in *Inelastic Ion-Surface Collisions,* edited by N. Tolk, J. C. Tully, W. Heiland, and C. W. White (Academic, New York, 1977).
[4]A. Blandin, A. Nourtier, and D. W. Hone, J. Phys. (Paris) 37, 369 (1976).
[5]J. K. Nørskov and B. I. Lundqvist, Phys. Rev. B 19, 5661 (1979).
[6]M. L. Yu, Phys. Rev. Lett. 47, 1325 (1981).
[7]N. D. Lang, Phys. Rev. B 27, 2019 (1983).
[8]A. R. Krauss and D. M. Gruen, Surf. Sci. 92, 14 (1980).
[9]T. R. Lundqvist, J. Vac. Sci. Technol. 15, 684 (1978).
[10]A. R. Bayley and R. J. MacDonald, Radiat. Eff. 34, 169 (1977).
[11]M. J. Vasile, Surf. Sci. Lett. 115, 141 (1982).
[12]Z. Sroubek, J. Zavadil, F. Kubec, and K. Zdansky, Surf. Sci. 77, 603 (1978).
[13]Z. Sroubek, K. Zdansky, and J. Zavadil, Phys. Rev. Lett. 45, 580 (1980).
[14]Z. Sroubek, Phys. Rev. B 25, 6046 (1982).
[15]R. A. Gibbs, S. P. Holland, K. E. Foley, B. J. Garrison, and N. Winograd, Phys. Rev. B 24, 6178 (1981).
[16]R. A. Gibbs, S. P. Holland, K. E. Foley, B. J. Garrison, and N. Winograd, J. Chem. Phys. 76, 684 (1982).
[17]P. H. Dawson and W. C. Tam, Surf. Sci. 91, 153 (1980).
[18]K. E. Foley and N. Winograd, Surf. Sci. 116, 1 (1982).
[19]A. Benninghoven, Surf. Sci. 53, 596 (1975).
[20]P. Sigmund, Phys. Rev. 184, 383 (1969).
[21]M. W. Thompson, Philos. Mag. 18, 377 (1968).
[22]P. Sigmund, in *Inelastic Ion-Surface Collisions,* Ref. 3, p. 121.
[23]H. Oechsner, Z. Phys. 288, 433 (1970).
[24]F. Bernhardt, H. Oechsner, and E. Stumpe, Nucl. Instrum. Methods 132, 329 (1976).
[25]R. B. Wright, M. J. Pellin, and D. M. Gruen, Surf. Sci. 110, 151 (1981).
[26]I. Reid, M. W. Thompson and B. W. Farmery, Radiat. Eff. 46, 163 (1980).
[27]R. A. Gibbs and N. Winograd, Rev. Sci. Instrum. 52, 1148 (1981).
[28]M. W. Siegel and M. J. Vasile, Rev. Sci. Instrum. 52, 1603 (1981).
[29]F. H. P. B. Habraken, E. Kieffer, and G. A. Bootsma, Surf. Sci. 83, 45 (1979).
[30]K. J. Snowdon and R. J. MacDonald, Int. J. Mass Spectrom. Ion Phys. 28, 233 (1978).
[31]R. G. Hart and C. B. Copper, Surf. Sci. 94, 105 (1980).
[32]A. R. Bayley and R. J. MacDonald, Radiat. Eff. 34, 169 (1977).
[33]A. V. Sidyakin, Zh. Eksp. Teor. Fiz. 58, 573 (1970) [Sov. Phys.—JETP, 31, 308 (1970)].
[34]H. Hagstrum, in *Inelastic Ion-Surface Collisions,* Ref. 2, p. 3.
[35]D. P. Eastman, Phys. Rev. B 2, 1 (1970).
[36]A. Cobas and W. E. Lamb, Phys. Rev. 65, 327 (1944).
[37]N. Matsunami, Y. Yamamura, Y. Itikawa, N. Itoh, Y. Kazumata, S. Miyagawa, K. Morita, and R. Shimizu (unpublished).